RESEARCH ARTICLE | DECEMBER 03 2025

Impact of graded doping transition layer on structural properties of Zr-doped AlN epilayers

H. Alwan ; D. Shima ; G. Balakrishnan ; J. Li ; J. Y. Lin ; H. X. Jiang

Appl. Phys. Lett. 127, 221905 (2025)
https://doi.org/10.1063/5.0305250
CHORUS

Impact of graded doping transition layer on structural properties of Zr-doped AlN epilayers

Cite as: Appl. Phys. Lett. **127**, 221905 (2025); doi: 10.1063/5.0305250
Submitted: 4 October 2025 · Accepted: 18 November 2025 ·
Published Online: 3 December 2025

H. Alwan,[1] D. Shima,[2] G. Balakrishnan,[2] J. Li,[1] J. Y. Lin,[1] and H. X. Jiang[1,a)]

AFFILIATIONS

[1]Department of Electrical and Computer Engineering, Texas Tech University, Lubbock, Texas 79409, USA
[2]Center for High Technology Materials, University of New Mexico, Albuquerque, New Mexico 87106, USA

[a)]Author to whom correspondence should be addressed: hx.jiang@ttu.edu

ABSTRACT

Zirconium doped AlN (AlN:Zr) epilayers hold significant promise for advanced electronic and quantum applications, including photoconductive semiconductor switches for high-voltage and high-power operations as well as quantum qubit and sensing technologies. Despite its potential, producing crack-free and high-quality AlN:Zr epilayers with high Zr concentrations has been challenging. The main obstacle is the significant atomic size difference between Zr and Al, which introduces a substantial lattice mismatch between the AlN:Zr epilayer and the AlN bulk substrate. This study investigates the impact of graded doping transition layer on structural and compositional properties of AlN:Zr by employing *in situ* doping using metal-organic chemical vapor deposition growth technique. Structural and compositional properties were analyzed in detail using x-ray diffraction (XRD), transmission electron microscopy, and energy dispersive spectroscopy. The implementation of the graded transition layer led to significant structural improvements, including reduced XRD linewidth, decreased threading dislocations, and lower concentrations of Al vacancies, and enabled the realization of a crack-free AlN:Zr epilayer with a high Zr doping concentration of 8.2×10^{20} cm^{-3}. These results demonstrate the effectiveness of the graded transition layer in producing high-quality AlN:Zr layers.

Group-III nitride semiconductors have revolutionized solid-state lighting and power electronics by enabling efficient light emitters and reliable high-power electronic devices such as inverters and converters.[1–6] III-nitride microLED has disrupted the high-resolution large-area flat panel display and 3D and augmented/virtual reality (AR/VR) display technologies.[7–10] The use of In-rich InGaN and Al-rich AlGaN alloys is also expanding into key areas including full-spectrum solar energy conversion, sterilization, and UV curing.[11–14]

AlN has an ultrawide bandgap (UWBG) around 6.1 eV.[15,16] Among III-nitrides, AlN possesses the highest value of critical field (E_C∼15 MV/cm),[17] high thermal conductivity (∼320 W/m·K),[18,19] and high electron mobility (>400 cm^2/V·s).[20] These properties make AlN highly attractive for deep UV optoelectronic devices operating near 200 nm[21,22] as well as for high-voltage/high-power electronic devices.[6,23] AlN also exhibits strong piezoelectric and electro-optic effects, enabling piezoelectric sensors operating at very high temperatures and in extreme environments[24] as well as integrated nonlinear photonic devices where AlN waveguides and resonators with low loss and high Q values have been demonstrated.[25] Beyond these applications, AlN has also emerged as a promising host for qubits and solid-state quantum emitters. First-principles studies have predicted that zirconium (Zr) dopant in AlN tends to substitute on the Al site (Zr_{Al}) and readily forms complexes with nitrogen vacancies (Zr_{Al}–V_N), which exhibit optically addressable spin-triplet ground states, similar to NV centers in diamond, making them an ideal candidate for quantum qubit.[26]

Experimental studies involving ion implantation have reported Zr-related optical emission lines in the 1.7–1.8 eV range, providing optical characterization results, which seem to be consistent with theoretical predictions.[27–29] However, ion implantation tends to severely degrade crystalline quality.[27–29] We recently demonstrated growth of Zr-doped AlN epilayers (AlN:Zr) by *in situ* doping using metal-organic chemical vapor deposition (MOCVD) with high crystalline quality and confirmed that Zr substitutes on Al site.[30,31] These epilayers exhibited strong sub-bandgap absorption and photoluminescence (PL) features attributed to the Zr_{Al}–V_N complex,[30,31] further supporting their role as optically active dopants for qubit applications. Moreover, such sub-bandgap absorption along with AlN's UWBG and exceptionally high critical field makes AlN:Zr particularly relevant for applications in photoconductive semiconductor switches (PCSSs) and

optically triggered electronic devices with superior performance over current existing technologies in terms of operating voltages, photocurrents, and switching jitter.[32–37] For these applications, a balance must be struck to achieve a suitable doping level without compromising performance. However, because the atomic size of Zr is larger than that of Al, the incorporation of Zr leads to cracks and increases threading dislocations and native defects, thereby degrading device performance. In this work, by implementing a graded doping transition layer, we demonstrate that a Zr doping level exceeding $10^{20}\,cm^{-3}$ can be achieved without compromising the crystalline quality of the top AlN:Zr active layer.

The approach of implementing a transition layer consisting of graded doping region has been adopted to produce erbium doped GaN (GaN:Er) epitaxial materials with improved crystalline quality.[38] Similarly, the effects of a compositionally graded buffer layer on stress evolution during GaN and $Al_xGa_{1-x}N$ MOCVD on SiC substrates have also been previously investigated.[39] In this work, undoped and Zr-doped AlN epilayers were grown by MOCVD on 2-inch diameter AlN bulk substrates (produced by physical vapor transport by Crystal IS). Trimethylaluminum (TMA) and ammonia (NH_3) were utilized as the Al and N precursors, respectively. Tetrakis (dimethylamino) zirconium {TDMAZr, $Zr[N(CH_3)_2]_4$} was employed as the Zr precursor, which was carried into the reactor using hydrogen gas.

We noted that the Zr doping concentration is not proportional to the flow rate of doping source but rather increases linearly with decreasing the growth rate of AlN. To implement a graded doping transition layer in the structure, we gradually ramp down the TMA flow rate in the graded doping region in five growth steps. As schematically illustrated in Fig. 1(a), the TMA flow rate was decreased from 100 standard cubic centimeter per minute (sccm) to 20 sccm in sequential steps while keeping the flow rate of Zr doping source at 400 ml/min to create a transition layer with Zr concentration progressively increasing toward the final AlN:Zr epilayer. The growth rate of the top active AlN:Zr epilayer was around 0.9 μm/h. This graded doping structure was designed to gradually change the Zr doping concentration by smoothing the transition in the lattice constant between the AlN bulk substrate and the top AlN:Zr epilayer. This prevents the abrupt changes that cause high stress concentrations, which can lead to cracking and threading dislocation generation and propagation.

Figure 1(b) plots the corresponding Zr concentration profile in the layer structure shown in Fig. 1(a), probed by secondary ion mass spectrometry (SIMS) measurements (performed by Charles Evans & Associates). The SIMS depth profile demonstrated the effective implementation of this approach and confirmed a gradual increase in Zr concentration from bottom to topmost AlN:Zr active layer, which consists of a Zr doping concentration as high as $8.2 \times 10^{20}\,cm^{-3}$.

X-ray diffraction (XRD) measurements were carried out to assess the effect of graded doping transition layer on the crystalline quality of AlN:Zr. The angular resolution of the XRD system used in this study is about 90 arcsec. Microstructural and compositional analyses were performed using a JEOL NEOARM 200CF atomic resolution aberration corrected scanning transmission electron microscope (STEM/TEM), equipped with a cold field emission gun (FEG) and ultrahigh-resolution pole piece. The instrument provides a point-to-point resolution of 0.19 nm in the TEM mode and a scanning STEM resolution of 71 pm, enabling high-fidelity imaging of dislocations, interfaces, and surface morphology. SEM and TEM modes were utilized to examine the surface features and cross-sectional microstructures of AlN and AlN:Zr epilayers. Selected-area electron diffraction (SAED) patterns were collected to evaluate epitaxial alignment and crystalline quality. Elemental analysis was carried out using the integrated JEOL SDD 100 mm^2 energy dispersive X-ray spectroscopy (EDS) detectors, supported by the Oxford Instruments Aztec software suite for full spectral mapping. High speed X-ray mapping was employed to extract Zr dopants incorporation profiles with nanometer scale spatial resolution. Line scans and 2D elemental maps revealed the distribution of Zr, Al, and N across the grading doping layer region. At the same time, background corrected quantification enabled direct comparison of dopant incorporation among AlN:Zr epilayers with and without the graded doping transition layer.

Figures 2(a) and 2(b) compare XRD patterns in ω-2θ scan and ω-scan (rocking curve) of the AlN (002) diffraction peak, and Fig. 2(c) compares TEM characterization results of (1) undoped AlN, (2) uniformly doped AlN:Zr epilayer, and (3) AlN:Zr epilayer incorporating a graded doping transition layer, all deposited on AlN substrates. The growth conditions of the topmost active AlN:Zr and AlN epilayers are identical. The ω–2θ scans reveal sharp diffraction peaks at $2\theta = 36.03°$ for all three samples due to the fact that the dominant XRD signal

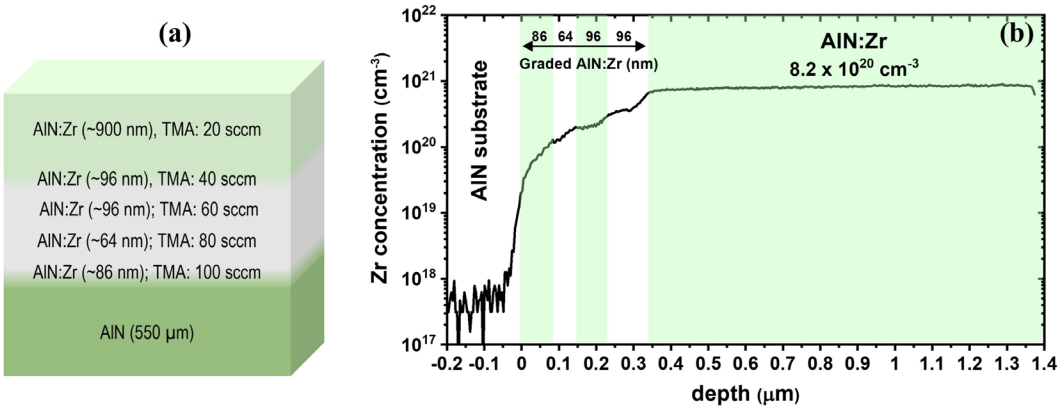

FIG. 1. (a) Schematic representation of layer structure of an AlN:Zr epilayer implementing a graded doping transition layer and (b) the corresponding Zr doping concentration profile probed by SIMS, showing a high Zr incorporation level of $8.2 \times 10^{20}\,cm^{-3}$ in the topmost active layer.

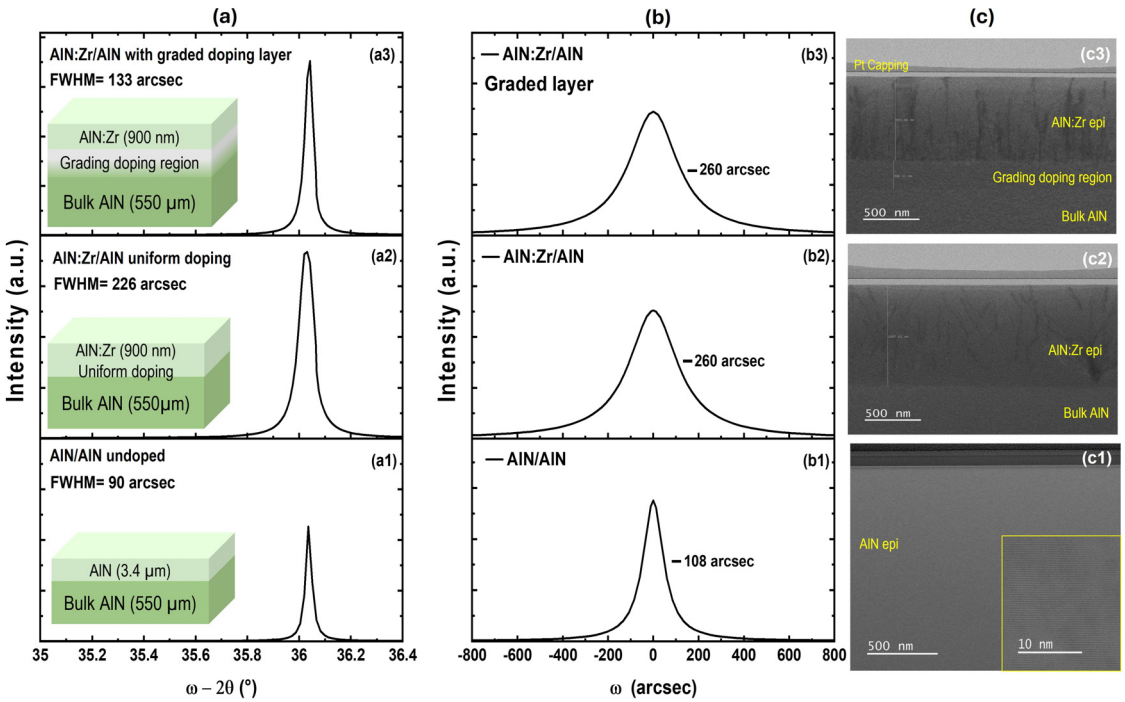

FIG. 2. XRD (ω-2θ, rocking curves) scans of the (002) peaks and cross-sectional TEM images of undoped AlN epilayer [(a1), (b1), and (c1)], uniformly doped AlN:Zr epilayer [(a2), (b2), and (c2)], and AlN:Zr epilayer with graded doping transition layer [(a3), (b3), and (c3)], all grown on AlN bulk substrates. The angular resolution of the XRD system is about 90 arcsec. A high-resolution TEM (HRTEM) image of undoped AlN is shown in the inset of (c1).

contributions are from AlN bulk substrates. Our earlier results revealed that the c-lattice constant of AlN:Zr exhibits a linear increase with Zr concentration, increasing from 4.980 Å in undoped AlN to 4.992 Å at $[Zr] \approx 1 \times 10^{20}\,cm^{-3}$, and this behavior arises from the substitution of larger Zr atoms onto the smaller Al sublattices,[30] leading to lattice mismatch between the AlN substrate and top active AlN:Zr epilayer and making the growth of AlN:Zr epilayers with high Zr concentrations difficult. Indeed, as shown in Figs. 2(a1) and 2(a2), the measured full width at half maximum (FWHM) value of the (002) peak is 90 arcsec (limited by our XRD system resolution) for undoped AlN epilayer and increases to 226 arcsec for uniformly doped AlN:Zr epilayer. In contrast, by incorporating a graded doping transition layer, the (002) peak FWHM of AlN:Zr epilayer decreases substantially to 133 arcsec, as shown in Fig. 2(a3), signifying a marked improvement in crystalline coherence and reduced strain within the lattice. The corresponding XRD rocking curves shown in Figs. 2(b1)–2(b3) demonstrate a clear difference in crystalline qualities among undoped AlN and Zr-doped AlN. The undoped AlN epilayer exhibits a FWHM of 108 arcsec, which is mostly limited by the resolution of the XRD system used in this study, as our previous results revealed a rocking curve FWHM of about 20 arcsec for undoped AlN epilayers deposited on sapphire.[30] In comparison, the rocking curve FWHMs of both AlN:Zr epilayers are broadened to 260 arcsec, reflecting an increase in the density of threading dislocations. The constant rocking curve FWHM of 260 arcsec indicates a similar density of screw dislocations in both types of AlN:Zr epilayer. Although no changes in the rocking curve FWHM were observed, the overall reduction in broadening of the symmetric ω–2θ scan demonstrates improved mosaic coherence and a decrease in edge dislocation density in AlN:Zr epilayer incorporating a graded doping transition layer. The results, therefore, highlight that the insertion of a graded doping transition layer enhances the structural quality of AlN:Zr epilayer. This interpretation is further supported by cross-sectional TEM results shown in Fig. 2(c) and discussed later.

Figure 2(c) highlights the contrast in microstructural quality between undoped AlN and AlN:Zr epilayers. The undoped AlN layer shown in Fig. 2(c1) exhibits a highly uniform and defect-free microstructure, with no visible extended defects in the examined cross-sectional TEM region. The high-resolution TEM (HRTEM) image shown in the inset of Fig. 2(c1) further reveals continuous lattice fringes extending across the epilayer, indicative of coherent epitaxial growth with a very low density of extended defects. This confirms our ability for producing AlN homoepilayers with excellent crystalline quality.[30] The cross-sectional TEM image for uniformly doped AlN:Zr sample shown in Fig. 2(c2), on the other hand, displays contrast variations and vertically aligned patterns that extend across the entire epilayer. These characteristics are consistent with dislocation and defect development brought on by Zr incorporation with many dislocations appearing to originate at the substrate/epilayer interface, though dislocations were also observable in the AlN bulk substrate. These characteristics point to stress-induced structural irregularities, stacking faults, or threading dislocations that spread throughout the epilayer due to lattice disruption brought on by Zr atoms replacing Al. Moreover, TEM image reveals the presence of cracks in the uniformly doped AlN:Zr epilayer. In contrast, in the case of AlN:Zr epilayer

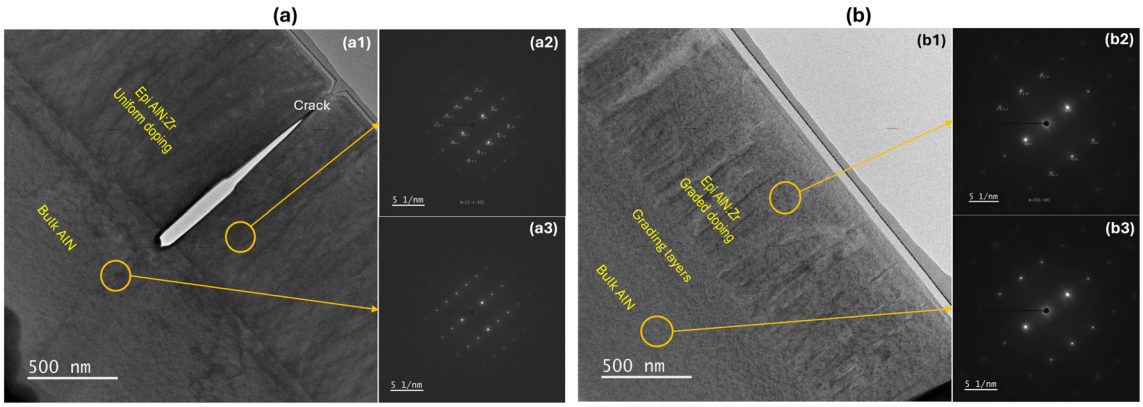

FIG. 3. Comparison of cross-sectional TEM images and selected-area electron diffraction (SAED) patterns among (a) uniformly doped AlN:Zr epilayer and (b) AlN:Zr epilayer with a graded doping transition layer, all grown on bulk AlN substrates. (a1) TEM image of a uniformly doped AlN:Zr epilayer, showing the interface between the epitaxial AlN:Zr and bulk AlN and (a2 and a3) the corresponding SAED patterns taken from the uniformly doped epilayer and bulk AlN. (b1) TEM image of an AlN:Zr epilayer with a graded doping transition layer inserted in between the AlN substrate and the topmost AlN:Zr epilayer, and (b2, b3) SAED patterns collected from the topmost AlN:Zr epilayer and bulk AlN.

incorporating graded doping shown in Fig. 3(a1), it is interesting to note that no defects are visible in the grading region, and dislocations seem to originate at the interface between the top grading and AlN:Zr layers. Overall, the number of threading dislocations in the AlN:Zr epilayer is significantly reduced by inserting a graded doping transition layer, as demonstrated by the comparison results shown in Figs. 2(c2) and 2(c3). These results confirm that the graded doping transition layer provides a viable pathway to achieve higher quality AlN:Zr epilayers by balancing high dopant incorporation with reduced defect density.

Figure 3 compares cross-sectional TEM images and selected-area electron diffraction (SAED) patterns among (a) uniformly doped AlN:Zr epilayer and (b) AlN:Zr epilayer with a graded doping transition layer. The SAED patterns for uniformly doped sample were taken perpendicular to the crack line for best imaging of the crack, along the direction of $[2\,\bar{1}\,\bar{1}\,0]$, whereas the sample with a graded doping transition layer was oriented to one of the cleaved sample edges, along the direction of $[01\,\bar{1}\,0]$. In the case of the direct growth of AlN:Zr layer without graded doping transition layer shown in Fig. 3(a), the interface between the AlN:Zr epilayer and the bulk AlN is very sharp, yet the selected-area electron diffraction (SAED) patterns obtained from both regions confirm the single crystalline nature of the epilayer and coherent epitaxial relationship with the substrate. However, contrast variations across the epilayer indicate the presence of strain accumulation when the graded doping transition layer is absent. On the other hand, in the sample incorporating a graded doping transition layer shown in Fig. 3(b), interface between the AlN substrate and graded doping layer and defects in the grading region are totally absent. The interface between AlN:Zr and graded doping transition layers is smoother, and the entire layer structure contains fewer strain contrast features. The results suggest more effective lattice accommodation at the boundary. The corresponding SAED patterns from both the AlN:Zr epilayer and the substrate confirm coherent epitaxy, with reduced evidence of misfit strain compared to the uniformly doped AlN:Zr epilayer.

XRD and TEM results together indicate that dislocation and defect generation and propagation are considerably inhibited by adding a graded doping transition layer with a total thickness of about 300 nm in between the AlN substrate and AlN:Zr epilayer. By allowing for a more gradual accommodation of lattice constant increase caused by Zr incorporation, the graded doping transition layer structure reduces the possibility of prolonged defect forming, which would otherwise degrade the crystalline quality. The resulting AlN:Zr epilayer above the grading doping layer appears structurally more uniform with no cracks.

STEM-EDS mapping was performed to analyze the elemental distribution in both uniformly doped AlN:Zr epilayer and AlN:Zr epilayer incorporating graded doping transition layer. In Fig. 4, elemental mapping images are shown for Zr only. For the AlN:Zr epilayer without graded doping transition layers shown in Fig. 4(a1), the Zr concentration exhibits a sharp increase at the AlN/AlN:Zr interface. The strain and stacking fault propagation seen in TEM studies are consistent with this abrupt shift. On the other hand, the integration profile of the AlN:Zr epilayer with a graded doping transition layer shown in Fig. 4(b1) is smoother, and the Zr distribution gradually increases over the grading region. This transition region is further supported by the EDS line profiles shown in Figs. 4(b1) and 4(b2), which reveal a gradual increase in Zr concentration in AlN:Zr epilayer with a graded doping transition layer [Fig. 4(b2)] as opposed to an abrupt jump in Zr concentration in uniformly doped AlN:Zr epilayer [Fig. 4(b1)].

It is also worth noting from the line profiles that relative to the AlN bulk substrate, Al contents are lower in both types of AlN:Zr epilayers, while the N content appears relatively constant, indicating the presence of Al vacancies (V_{Al}) in Zr-doped epilayers. Because Zr substitutes on the Al site and acts as a donor, the incorporation of Zr is expected to shift the Fermi level toward the conduction band edge during growth, likely resulting in a reduction in the formation energy of V_{Al}.[40] However, carefully inspecting the EDS line profiles, Al deficiency is less severe in AlN:Zr epilayer, incorporating a graded doping transition layer compared to the uniformly doped AlN:Zr. Although EDS measurements cannot provide quantitative concentrations, the Al/N ratios estimated from the EDS profiles are approximately 0.90

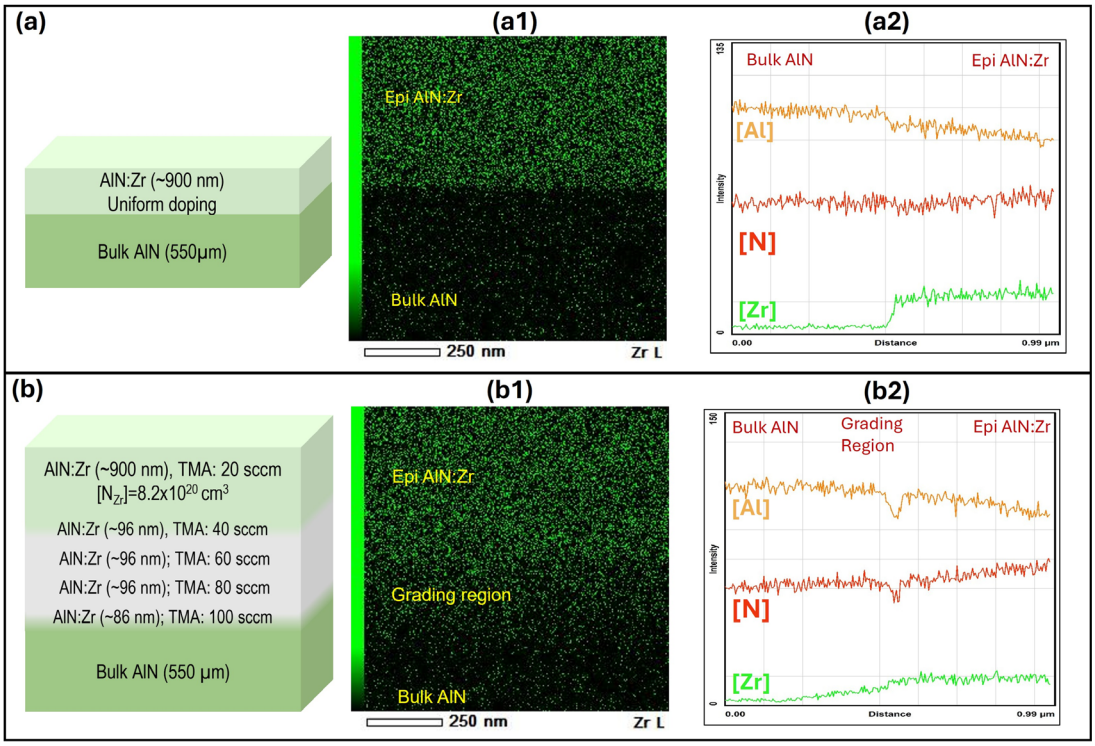

FIG. 4. STEM-EDS elemental mapping results of (a1) uniformly doped AlN:Zr epilayer, showing a sharp Zr onset at the interface and (b1) AlN:Zr epilayer with graded doping transition layer revealing a smoother Zr transition across the grading region.

and 0.94, respectively, in uniformly doped and grading doped AlN:Zr epilayers by assuming the Al/N ratio is 1/1 in the AlN bulk substrate. Al vacancies in AlN are free electron traps, and their presence is detrimental for many device applications.[40] In addition to the XRD and TEM data showing enhanced structural coherence, the results shown in Figs. 4(a2) and 4(b2) confirm that the smoother integration of Zr dopants also reduces doping induced V_{Al}, making the graded doping transition layer approach advantageous for engineering AlN:Zr layer structures.

In summary, the crack-free Zr-doped AlN epitaxial layer with a Zr doping concentration as high as $8.2 \times 10^{20}\,\mathrm{cm}^{-3}$ was produced on AlN bulk substrates by *in situ* doping using MOCVD technique, and their structural and compositional properties have been characterized. A graded doping transition layer strategy was proved highly effective at suppressing strain accumulation at the AlN:Zr/AlN interface and within the AlN:Zr epilayer itself. Complementary STEM-EDS mapping demonstrated the desired gradual and well-controlled Zr incorporation in the graded region, a sharp contrast to the abrupt Zr profile observed in the uniformly doped AlN:Zr epilayer. Cross-sectional TEM measurement results confirmed a significant reduction in the generation and propagation of dislocations in the AlN:Zr epilayer when incorporating the graded doping, compared to layers with uniform doping. The graded doping also led to a reduced presence of Al vacancies in the AlN:Zr epilayer. These are promising results to guide the growth of highly doped AlN:Zr epilayers with high crystalline quality for emerging device applications.

The information, data, or work presented herein was funded in part by the Advanced Research Projects Agency-Energy (ARPA-E), U.S. Department of Energy, under ULTRAFAST program, Award No. DE-AR0001821, monitored by Dr. Johan Enslin, Dr. Olga Spahn, and Dr. Eric Carlson. Electron microscopy was carried out in the Nanomaterials Characterization Facility at the University of New Mexico, a facility that is supported by the State of New Mexico, the National Science Foundation, and the National Aeronautics and Space Administration. The acquisition of the JEOL NEOARM AC-S/TEM at the University of New Mexico was supported by NSF Grant DMR-1828731 and NASA Emerging Worlds Grant 80NSSC21K1757. The views and opinions of authors expressed herein do not necessarily state or reflect those of the United States Government or any agency thereof. Jiang and Lin are grateful to the AT&T Foundation for the support of Ed Whitacre and Linda Whitacre endowed chairs.

AUTHOR DECLARATIONS

Conflict of Interest

The authors have no conflicts to disclose.

Author Contributions

H. Alwan: Data curation (equal); Formal analysis (equal); Investigation (equal); Methodology (equal); Software (equal); Validation (equal); Visualization (equal); Writing – original draft

(equal). **D. Shima:** Data curation (equal); Formal analysis (equal); Investigation (equal); Methodology (equal); Software (equal); Validation (equal); Visualization (equal); Writing – review & editing (equal). **G. Balakrishnan:** Data curation (equal); Formal analysis (equal); Investigation (equal); Methodology (equal); Software (equal); Validation (equal); Visualization (equal); Writing – review & editing (equal). **J. Li:** Data curation (equal); Formal analysis (equal); Investigation (equal); Methodology (equal); Project administration (equal); Resources (equal); Software (equal); Supervision (equal); Validation (equal); Visualization (equal). **J. Y. Lin:** Conceptualization (equal); Data curation (equal); Formal analysis (equal); Funding acquisition (equal); Investigation (equal); Methodology (equal); Project administration (equal); Resources (equal); Software (equal); Supervision (equal); Validation (equal); Visualization (equal); Writing – review & editing (equal). **H. X. Jiang:** Conceptualization (equal); Formal analysis (equal); Funding acquisition (equal); Investigation (equal); Methodology (equal); Project administration (equal); Resources (equal); Supervision (equal); Validation (equal); Visualization (equal); Writing – review & editing (equal).

DATA AVAILABILITY

The data that support the findings of this study are available within the article.

REFERENCES

[1]H. Amano, N. Sawaki, I. Akasaki, and Y. Toyoda, "Metalorganic vapor phase epitaxial growth of a high quality GaN film using an AlN buffer layer," Appl. Phys. Lett. **48**, 353 (1986).

[2]S. Nakamura, T. Mukai, and M. Senoh, "Candela-class high-brightness InGaN/AlGaN double-heterostructure blue-light-emitting diodes," Appl. Phys. Lett. **64**, 1687 (1994).

[3]M. Asif Khan, A. Bhattarai, J. N. Kuznia, and D. T. Olson, "High electron mobility transistor based on GaN-AlGaN heterojunction," Appl. Phys. Lett. **63**, 1214 (1993).

[4]H. Amano, Y. Baines, E. Beam *et al.*, "The 2018 GaN power electronics roadmap," J. Phys. D: Appl. Phys. **51**, 163001 (2018).

[5]Y. Xu, V. G. T. Vangipuram, V. Talesara, J. Cheng, Y. Zhang, T. Hashimoto, E. Letts, D. Key, H. Zhao, and W. Lu, "7.86 kV GaN-on-GaN PN power diode with $BaTiO_3$ for electrical field management," Appl. Phys. Lett. **123**, 142105 (2023).

[6]Y. H. Chen, J. Encomendero, C. Savant, V. Protasenko, H. G. Xing, and D. Jena, "Electron mobility enhancement by electric field engineering of AlN/GaN/AlN quantum-well HEMTs on single-crystal AlN substrates," Appl. Phys. Lett. **124**, 152111 (2024).

[7]S. X. Jin, J. Li, J. Z. Li, J. Y. Lin, and H. X. Jiang, "GaN microdisk light emitting diodes," Appl. Phys. Lett. **76**, 631 (2000).

[8]J. Day, J. Li, D. Y. C. Lie, C. Bradford, J. Y. Lin, and H. X. Jiang, "III-nitride full-scale high-resolution microdisplays," Appl. Phys. Lett. **99**, 031116 (2011).

[9]H. X. Jiang and J. Y. Lin, "How we made the microLED," Nat. Electron. **6**, 257 (2023).

[10]P. J. Parbrook, B. Corbett, J. Han, T. Y. Seong, and H. Amano, "Micro-light emitting diode: From chips to applications," Laser Photonics Rev. **15**, 2000133 (2021).

[11]J. Wu, W. Walukiewicz, K. Yu, J. W. Ager III, E. E. Haller, H. Lu, W. J. Schaff, Y. Saito, and Y. Nanishi, "Small band gap bowing in InGaN alloys," Appl. Phys. Lett. **80**, 4741 (2002).

[12]S. Vanka, B. Zhou, R. A. Awni, Z. Song, F. A. Chowdhury, X. Liu, H. Hajibabaei, W. Shi, Y. Xiao, I. A. Navid, A. Pandey, R. Chen, G. A. Botton, T. W. Hamann, D. Wang, Y. Yan, and Z. Mi, "InGaN/Si double-junction photocathode for unassisted solar water splitting," ACS Energy Lett. **5**, 3741 (2020).

[13]M. A. Khan, K. Balakrishnan, and T. Katona, "Ultraviolet light-emitting diodes based on group three nitrides," Nat. Photonics **2**, 77 (2008).

[14]Z. Zhang, M. Kushimoto, T. Sakai, N. Sugiyama, L. J. Schowalter, C. Sasaoka, and H. Amano, "A 271.8 nm deep-ultraviolet laser diode for room temperature operation," Appl. Phys. Express **12**, 124003 (2019).

[15]P. B. Perry and R. F. Rutz, "The optical absorption edge of single-crystal AlN prepared by a close-spaced vapor process," Appl. Phys. Lett. **33**, 319 (1978).

[16]J. Li, K. B. Nam, M. L. Nakarmi, J. Y. Lin, H. X. Jiang, P. Carrier, and S.-H. Wei, "Band structure and fundamental optical transitions in wurtzite AlN," Appl. Phys. Lett. **83**, 5163 (2003).

[17]T. L. Chu and R. W. Kelm, "The preparation and properties of aluminum nitride films," J. Electrochem. Soc. **122**, 995 (1975).

[18]G. A. Slack, "Nonmetallic crystals with high thermal conductivity," J. Phys. Chem. Solids **34**, 321 (1973).

[19]R. L. Xu, M. M. Rojo, S. M. Islam, A. Sood, B. Vareskic, A. Katre, N. Mingo, K. E. Goodson, H. G. Xing, D. Jena, and E. Pop, "Thermal conductivity of crystalline AlN and the influence of atomic-scale defects," J. Appl. Phys. **126**, 185105 (2019).

[20]Y. Taniyasu, M. Kasu, and T. Makimoto, "Increased electron mobility in *n*-type Si-doped AlN by reducing dislocation density," Appl. Phys. Lett. **89**, 182112 (2006).

[21]Y. Taniyasu, M. Kasu, and T. Makimoto, "An aluminium nitride light-emitting diode with a wavelength of 210 nanometres," Nature **441**, 325 (2006).

[22]J. Li, Z. Y. Fan, R. Dahal, M. L. Nakarmi, J. Y. Lin, and H. X. Jiang, "200 nm deep ultraviolet photodetectors based on AlN," Appl. Phys. Lett. **89**, 213510 (2006).

[23]W. A. Doolittle, C. M. Matthews, H. Ahmad, K. Motoki, S. Lee, A. Ghosh, E. N. Marshall, A. L. Tang, P. Manocha, and P. D. Yoder, "Prospectives for AlN electronics and optoelectronics and the important role of alternative synthesis," Appl. Phys. Lett. **123**, 070501 (2023).

[24]N. I. Kim, M. Yarali, M. Moradnia, M. Aqib, M. H. Ji, V. S. Parameshwaran, A. Sampath, C.-H. Liao, F. AlQatari, M. Nong, X. Li, and J. H. Ryou, "Piezoelectric sensors operating at very high temperatures and in extreme environments made of flexible ultrawide-bandgap single-crystalline AlN thin films," Adv. Funct. Mater. **33**, 2212538 (2023).

[25]X. Guo, C.-L. Zou, and H. X. Tang, "Second-harmonic generation in aluminum nitride microrings with 2500%/W conversion efficiency," Optica **3**, 1126 (2016).

[26]J. B. Varley, A. Janotti, and C. G. Van de Walle, "Defects in AlN as candidates for solid-state qubits," Phys. Rev. B **93**, 161201(R (2016).

[27]A. Aghdaei, R. Pandiyan, B. Ilahi, M. Chicoine, M. E. Gowini, F. Schiettekatte, L. G. Fréchette, and D. Morris, "Engineering visible light emitting point defects in Zr-implanted polycrystalline AlN films," J. Appl. Phys. **128**, 245701 (2020).

[28]A. Senichev, Z. O. Martin, Y. Wang, O. M. Matthiessen, A. Lagutchev, H. Htoon, A. Boltasseva, and V. M. Shalaev, "Quantum emitters in aluminum nitride induced by heavy ion irradiation," APL Quantum **1**, 036103 (2024).

[29]T. Yokoyama, Y. Iwazaki, Y. Onda, T. Nishihara, Y. Sasajima, and M. Ueda, "Effect of Mg and Zr co-doping on piezoelectric AlN thin films for bulk acoustic wave resonators," IEEE Trans. Ultrason., Ferroelectr., Freq. Control **61**, 1322 (2014).

[30]H. Alwan, N. K. Hossain, J. Li, J. Y. Lin, and H. X. Jiang, "Growth and characterization of high-quality Zr doped AlN epilayers," Appl. Phys. Lett. **126**, 022106 (2025).

[31]H. Alwan, M. Almohammad, J. Li, J. Y. Lin, and H. X. Jiang, "Optical properties of Zr-doped AlN epilayers," APL Mater. **13**, 071115 (2025).

[32]J. Huang, L. Hu, X. Yang, Y. Sun, X. Li, and C. Liu, "Modeling and simulation of Fe-doped GaN PCSS in high-power microwave," IEEE Trans. Electron Devices **70**, 3489 (2023).

[33]A. D. Koehler, T. J. Anderson, A. Khachatrian, A. Nath, M. J. Tadjer, S. P. Buchner, K. D. Hobart, and F. J. Kub, "High voltage GaN lateral photoconductive semiconductor switches," ECS J. Solid State Sci. Technol. **6**, S3099 (2017).

[34]E. Majda-Zdancewicz, M. Suproniuk, M. Pawłowski, and M. Wierzbowski, "Current state of photoconductive semiconductor switch engineering," Opto-Electron. Rev. **26**, 92 (2018).

[35]J. Leach, R. Metzger, E. Preble, and K. Evans, "High voltage bulk GaN-based photoconductive switches for pulsed power applications," Proc. SPIE **8625**, 86251Z (2013).
[36]J. S. Sullivan and J. R. Stanley, "Wide bandgap extrinsic photoconductive switches," IEEE Trans. Plasma Sci. **36**, 2528 (2008).
[37]K. Zhu, S. Doğan, Y. Moon, J. Leach, F. Yun, D. Johnstone, H. Morkoç, G. Li, and B. Ganguly, "Effect of n^+-GaN subcontact layer on 4H–SiC high-power photoconductive switch," Appl. Phys. Lett. **86**, 261108 (2005).
[38]Z. Y. Sun, Y. Q. Yan, T. B. Smith, W. P. Zhao, J. Li, J. Y. Lin, and H. X. Jiang, "Growth and fabrication of GaN/Er:GaN/GaN core-cladding planar waveguides," Appl. Phys. Lett. **114**, 222105 (2019).
[39]J. D. Acord, X. Weng, E. C. Dickey, D. W. Snyder, and J. M. Redwing, "Effects of a compositionally graded buffer layer on stress evolution during GaN and $Al_xGa_{1-x}N$ MOCVD on SiC substrates," J. Cryst. Growth **310**, 2314 (2008).
[40]C. Stampfl and C. G. Van de Walle, "Theoretical investigation of native defects, impurities, and complexes in aluminum nitride," Phys. Rev. B **65**, 155212 (2002).